

D. Stoyanov, M. Beurskens, T. Dreischuh, L. Gurdev, O. Ford, J. Flanagan,
M. Kempenaars, I. Balboa, M. Walsh and JET EFDA contributors

Resolving the Plasma Electron Temperature Pedestal in JET from Thomson Scattering Core LIDAR Data

“This document is intended for publication in the open literature. It is made available on the understanding that it may not be further circulated and extracts or references may not be published prior to publication of the original when applicable, or without the consent of the Publications Officer, EFDA, Culham Science Centre, Abingdon, Oxon, OX14 3DB, UK.”

“Enquiries about Copyright and reproduction should be addressed to the Publications Officer, EFDA, Culham Science Centre, Abingdon, Oxon, OX14 3DB, UK.”

The contents of this preprint and all other JET EFDA Preprints and Conference Papers are available to view online free at www.iop.org/Jet. This site has full search facilities and e-mail alert options. The diagrams contained within the PDFs on this site are hyperlinked from the year 1996 onwards.

Resolving the Plasma Electron Temperature Pedestal in JET from Thomson Scattering Core LIDAR Data

D. Stoyanov¹, M. Beurskens², T. Dreischuh¹, L. Gurdev¹, O. Ford², J. Flanagan²,
M. Kempenaars², I. Balboa², M. Walsh² and JET EFDA contributors*

JET-EFDA, Culham Science Centre, OX14 3DB, Abingdon, UK

¹*Institute of Electronics, Bulgarian Academy of Sciences and EURATOM/INRNE Fusion Association,
72 Tzarigradsko Shosse, Sofia, Bulgaria*

²*EURATOM/CCFE Fusion Association, Culham Science Centre, OX14 3DB, Abingdon, OXON, UK*

** See annex of F. Romanelli et al, "Overview of JET Results",
(Proc. 22nd IAEA Fusion Energy Conference, Geneva, Switzerland (2008)).*

Preprint of Paper to be submitted for publication in Proceedings of the
37th EPS Conference on Plasma Physics, Dublin, Ireland.
(21st June 2010 - 25th June 2010)

One of the basic strengths of the JET core LIDAR Thomson scattering system (Fig.1) is its potential to measure electron temperature T_e and density n_e profiles simultaneously along the entire line of sight inside the torus. Its spatial resolution of 12cm suffices to resolve the global profile shape, but does not allow the visualization of small scale structures such as the narrow edge pedestal area, which has a typical length scale of 2-3cm. Enhancement of the system's resolving power can be obtained by applying a deconvolution to each of the signals from the 6 spectral channels using the system's instrument function, as has been demonstrated in [1]. However, the data improvement using this technique has been limited by the necessary application of a low pass filter $H(r)$ in the deconvolution algorithm in order to keep the deconvolved noise below a tolerable level, which in turn leads to an incomplete reconstruction of the 'true' LIDAR profile $L_p^{true}(r)$. The thus obtained enhanced spectral signals are given by:

$$L_p^{dcv}(r) = L_p^{true}(r) \otimes H(r) + \tilde{W}_p^{dcv}(r), \quad (1)$$

where $L_p^{dcv}(r)$ are the deconvolved signals in the $p = 1..6$ spectral channels, $\tilde{W}_p^{dcv}(r)$ is the residual noise for each channel, r is a line-of-sight coordinate, and \otimes denotes convolution. The requirements to this low pass filter could be reduced by upgrading certain hardware components within the system. For example, it has been shown that improvements to both the spatial resolution and the Signal to Noise Ratio (SNR) can be obtained by replacing the existing detectors with faster and more sensitive GaAsP detectors [2]. This work has also shown that in addition upgrading the existing digitizer from a 1GHz bandwidth device with 5GSa/s to a 4 GHz bandwidth, 20GSa/s will reduce the overall system resolution to a 7cm at a three-fold improvement of the SNR [2]. This would reduce the need for $H(r)$, but still not fully eliminate it.

Further improvements in the deconvolution algorithm are presented here for finer estimation of the true T_e pedestal, assuming a well known filter characteristic $H(r)$. The approach is intended for application after upgrading the LIDAR receiving system with novel detectors and digitizers. However, the results presented and discussed here pertain to preliminary tests of this approach using the present core LIDAR data (spatial sampling step of 3cm). The optimal performance of the algorithm requires a smaller LIDAR data sampling step ≤ 1 cm. To this end, we applied an original algorithm [3] for transforming the LIDAR profiles to a finer spatial step of 1cm. Using this method, time averaged pedestals with a minimum time resolution of 1s (4 laser shots at 4Hz) can be resolved. Single shot performance can be achieved after upgrading the core LIDAR hardware without using the method in [3].

The block-schematic of the performance of this approach (Fig.2) includes two novel blocks. In block 1, LIDAR profiles are transformed to a 1cm sampling step [3]. Following this, the convolved and deconvolved T_e profiles are retrieved and further used for resolving the T_e pedestal via the optimal algorithm (block 2). This algorithm is the key algorithm here.

The method in block 1 is based on the lack of synchronization between the laser pulse and the

sampling generator, resulting in some time delays within one sampling step of the acquired profiles with respect to the laser emission. These delays, which contain information about the fine structure of the LIDAR profiles in the pedestal area, are estimated from the sampled LIDAR data assuming (for these preliminary test purposes) stationary behavior over the H-plasma mode. The LIDAR profiles are then subsequently rearranged onto the finer time scale, taking into account the above time delays that are preliminary divided into Q groups. Thus, the new sampling step will be Q -times as small as the former one or $\delta r = 1\text{cm}$, if $Q = 3$.

The basic parameters of the electron temperature pedestal used here are as follows: $S_{ped}^{norm}(r)$ normalized pedestal shape; A_{ped} – pedestal amplitude; W_{ped} – pedestal width; r_{ped} – upper pedestal position. The aim here is to create a model of the electron temperature profile $T_e^{var}(r)$ with variable pedestal parameters. The true T_e profile outside the pedestal area is assumed to be identical to the convolved profile $T_e^{con}(r)$. As such, the variable profile $T_e^{var}(r)$ can be further convolved with $H(r)$, which is preliminarily defined within the deconvolution [see Eq.1]. The smoothed variable temperature profile is denoted by $T_e^{var}(r, H(r))$. For each set of pedestal parameters, the functional F_{lsf} is then given by the expression:

$$F_{lsf} = \sum_{r \in ped.area} [T_e^{dcv}(r) - T_e^{var}(r, H(r))]^2 \quad (2)$$

The functional F_{lsf} has a minimum when $T_e^{var}(r, H(r)) \rightarrow T_e^{dcv}(r)$. As an estimate of the true T_e profile with a range-resolved pedestal, the profile $T_e^{var}(r)$ with pedestal parameters corresponding to the minimum of the functional F_{lsf} in (2) may be used. The problem formulated by (2) provides an optimal estimate of the T_e profile. By finding the optimal pedestal parameters, the entire T_e profile in the torus over the entire plasma sounding path can be restored. As a result, the information extracted from the core LIDAR data in the region of the plasma T_e pedestal can be significantly improved.

The results of simulations using the core LIDAR parameters confirm the good performance of this method at $SNRs \sim 20$ that are typical in H-mode, high-triangularity plasmas. Some example results for T_e profiles (averaged over 25 shots) are given in Fig.3 where curve 1 shows the input T_e profile and curves 2 and 3 show the convolved and the deconvolved profiles, respectively. As can be seen, the retrieved estimate of the input profile (curve 4) is closely coincident with curve 1. Moreover, the convolved by $H(r)$ retrieved profile (curve 5) overlaps well (as can be expected) with curve 3, which corresponds to the minimum of the functional in (2). The deviations of the retrieved pedestal widths for input pedestal widths ranging from 1.8cm to $\sim 5\text{cm}$ are given in Fig.4. It can be seen that the retrieved pedestal widths vary by $\pm 1\text{cm}$ with respect to the input pedestal widths.

Figures 5(a) and (b) show some preliminary results from the application of this method to core LIDAR data for JET pulses of different triangularity, together with validated T_e profiles from the JET High Resolution Thomson Scattering (HRTS). The resolved mean T_e profiles using the novel algorithm are presented by curves 2. The curves 1 are the HTRS T_e data, while curves 3 show the fitted curves to the HRTS data. It can be seen that the T_e pedestals are well defined by both the core

LIDAR (curve 2) and the HRTS system (curves 1 and 3) T_e profiles. The pedestal shapes retrieved by the novel algorithm also agree well with the fitted HRTS profiles. The statistics over 15 processed JET pulses displays differences below $\pm 1\text{cm}$ in estimates of the mean pedestal widths determined by both techniques. Moreover, the pedestal amplitudes match those from the HRTS fitted data to within $\pm 0.2\text{keV}$. Thus, good consistency is displayed between the pedestal parameters estimated by both techniques.

CONCLUSIONS

In conclusion, this paper presents a successful approach of resolving the mean T_e pedestal profiles within JET plasmas using data from the core LIDAR diagnostic. Significant further improvement of this approach should be possible when combined with the upgrades to the core LIDAR system discussed here, which should enable single shot pedestal analysis.

ACKNOWLEDGEMENTS.

This work, carried out under the EFDA, has been supported by the European Communities under the Contract of Association between EURATOM and INRNE (Bulgaria) and by the Bulgarian National Science Fund (contract F-1020). The views and opinions expressed herein do not necessarily reflect those of European Commission.

REFERENCES:

- [1]. D. Stoyanov et al., 36th EPS Conf. Plasma Physics, ECA Vol.33E, P-2.155 (2009).
- [2]. M. Kempnaars et al., Int.Conf. Plasma Diagnostics., France, 12-16 April 2010.
- [3]. D. Stoyanov et al., Measurement Science Technology **15**, 2361 (2004).

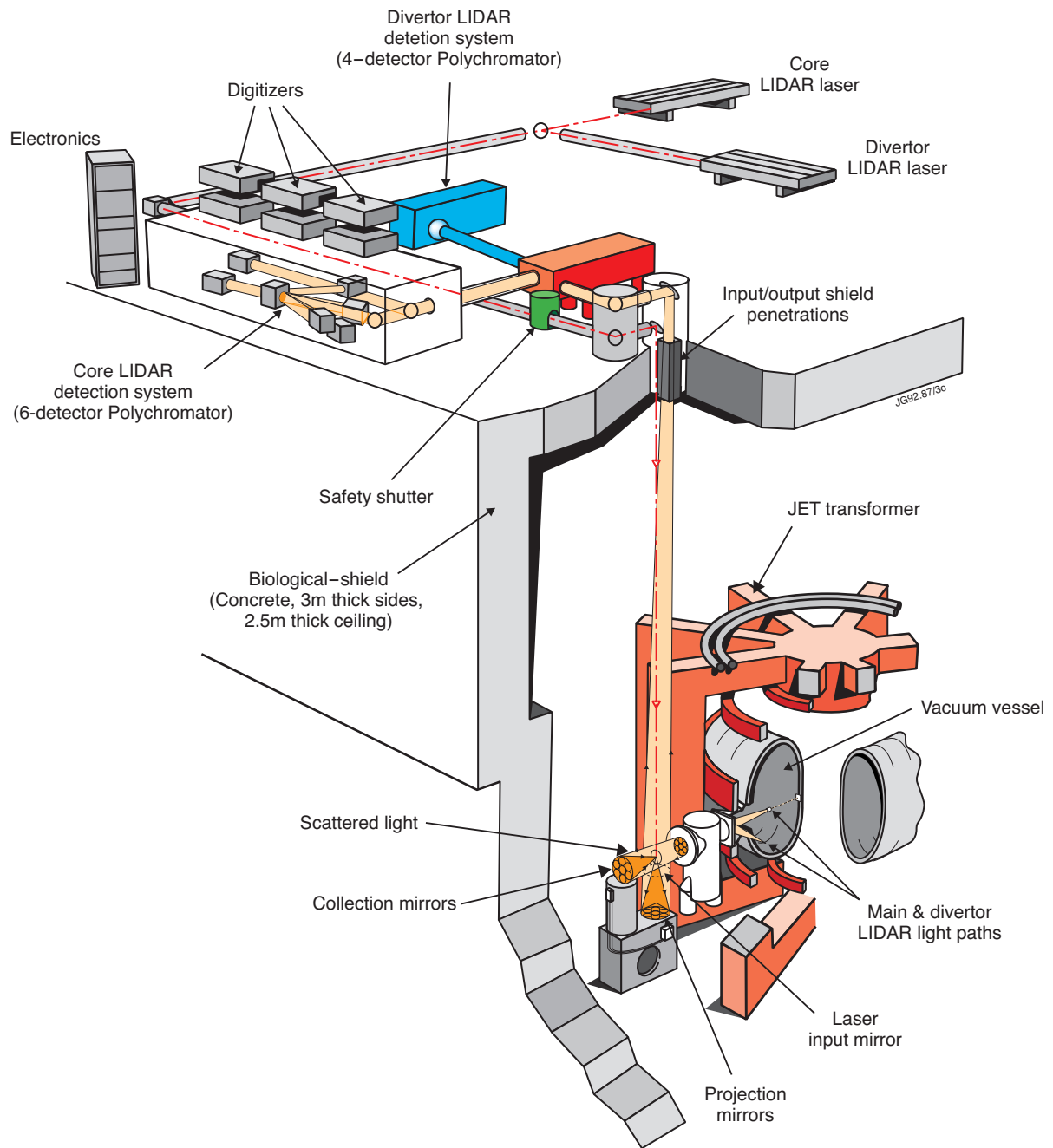


Figure 1:

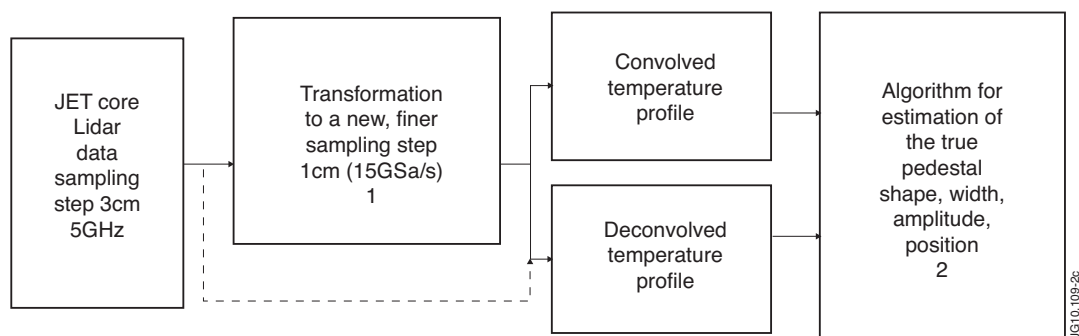


Figure 2:

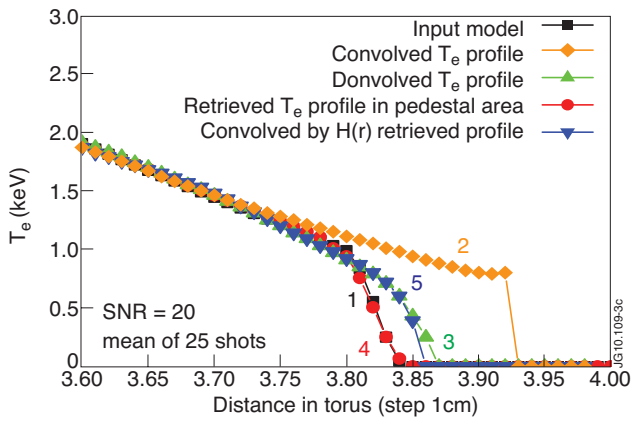


Figure 3:

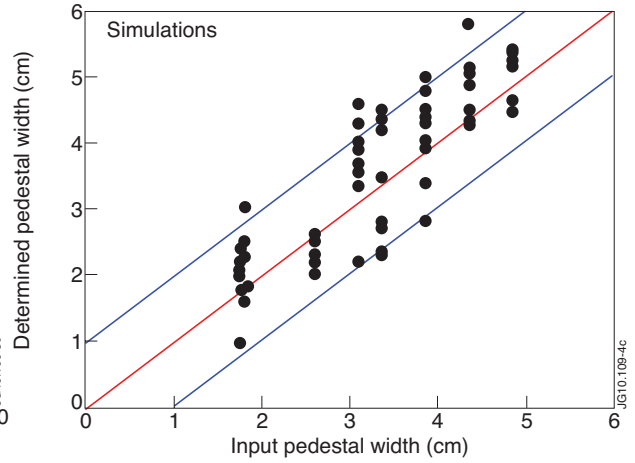


Figure 4:

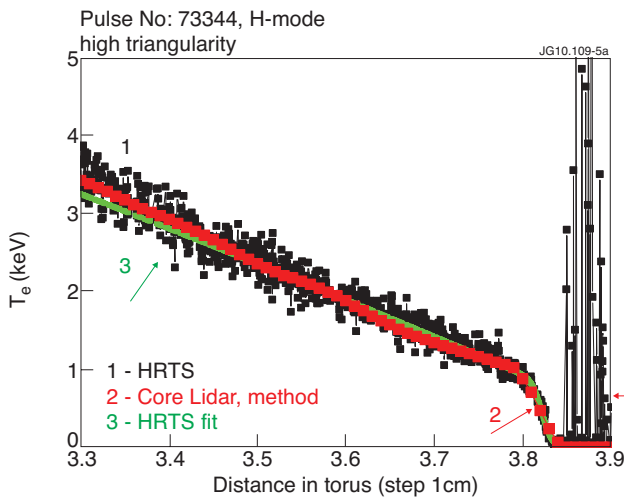


Figure 5a:

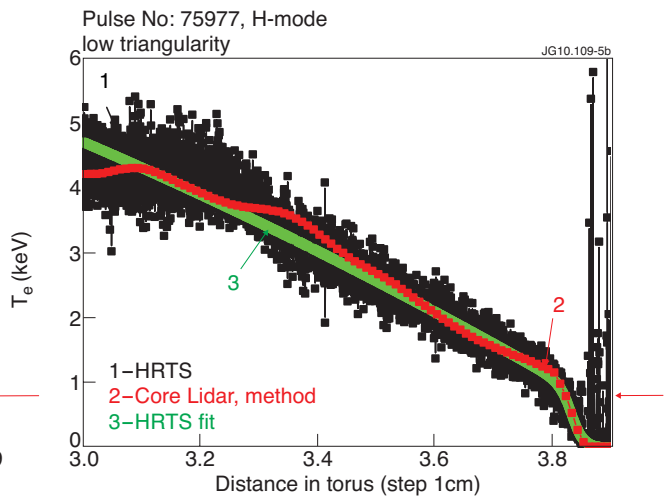


Figure 5b: